Improvement of the Hilbert Method via ESPRIT for Detecting Rotor Fault in Induction Motors at Low Slip

Boqiang Xu, *Member, IEEE*, Liling Sun, Lie Xu, *Senior Member, IEEE*, and Guoyi Xu

***Abstract*—The traditional Hilbert method to detect broken rotor bar fault in induction motors is reviewed and its major drawbacks are clearly revealed, namely, deteriorating or even completely failing when a motor operating at low slip due to the fixed constraints of fast Fourier transform (FFT) is used in this method. To overcome this, the estimation of signal parameters via rotational invariance technique (ESPRIT) is then introduced to replace FFT, and an improved Hilbert method is thus presented by conjugating the Hilbert transform and ESPRIT together. Experimental results of a small motor in a laboratory and a large motor operating on an industrial site are reported to demonstrate the effectiveness of the improved Hilbert method.**

***Index Terms*—Broken rotor bar, detection, estimation of signal parameters via rotational invariance technique (ESPRIT), Hilbert transform (HT), induction motor.**

I. Introduction

INDUCTION motors are used in a wide variety of industry applications including some very harsh environments, e.g., mining, steel plants, etc. Such operating environments make them susceptible to failures, and surveys have reported that broken rotor bar fault (BRB) constitutes approximately 10% of all the failures in induction motors [1]. As a result of this, it is of great significance to detect BRB earlier so as to allow the motors to be shut down in a controlled manner.

It has been widely established that once BRB occurred, harmonic components are induced in the stator current at frequencies given by $(1 \pm 2ks)f_1$, where s is the slip, f_1 is the supply frequency, and $k = 1, 2\ldots$ [2], [3]. This indicates that the $(1 \pm 2ks)f_1$ components in the stator current can be used as the BRB indicator. Thus, motor current signature analysis (MCSA) has been widely used in recent years and has become the benchmark procedure for BRB detection. With MCSA, the stator current is normally analyzed using fast Fourier transform (FFT) in order to yield the related information of the $(1 \pm 2ks)f_1$ and f_1 components [4]–[10]. However, the industrial application of MCSA has some practical limitations, explained as follows.

As the method is heavily dependent on the accuracy of FFT, it suffers from spectral leakage due to limited measurement data. It is well known that the $(1 \pm 2ks)f_1$ components are so small in magnitude with respect to the f_1 component (only a few percentages) that they can be easily buried by the latter's leaked energy. Consequently, the BRB detection performance deteriorates in real application, and occasionally the analysis can be completely erroneous, which has been reported in [6]–[9]. Various solutions have been proposed in [6] and [7] to minimize the spectral leakage and highlight the $(1 \pm 2ks)f_1$ components by filtering out the f_1 component before FFT is performed.

Spectral leakage has a special adverse impact when the motor operates at low slip because the $(1 \pm 2ks)$ f_1 and f_1 components are very close in the spectrum in this case, and hence, it is very difficult to separate them correctly. Therefore, a high-frequency resolution (inversely proportional to the measurement time) is required for a precise separation. This leads to a long measurement time which inevitably includes the variations of stator current and slip. Consequently, this results in the $(1 \pm 2ks)f_1$ components varying in both amplitude and frequency and, thus, degrades the BRB detection, as has been reported in [7], [9], and [11]. This implies that the steady-state condition, required for guaranteeing FFT accuracy, does not exist in reality. As a result of this, the FFT accuracy will be reduced too much to separate the components of interest in the spectrum. Alternative techniques such as Subdivision FFT [6], Zoom FFT [12], and discrete wavelet transformation (DWT) [13], [14], which generate spectra with more densely spaced frequency points, have been proposed to enhance frequency resolution without prolonging the measurement time.

Unfortunately, all the aforementioned methods become inefficient in the case of low slip because of unsatisfactory spectral leakage depression and/or a long measurement time. However, detecting BRB at low slip is very important in industry as large motors, widely used in industrial applications and needed to be frequently monitored, usually operate at low slip (less than 0.01 in common sense even at rated load). In fact, the problem of detecting BRB at low slip has become a bottle-neck nowadays preventing the wide use of BRB detection in industry, and thus needs to be addressed urgently.

The problem was addressed in [15], probably for the first time, with the so-called Hilbert method. The Hilbert transform (HT) was used to obtain the Hilbert modulus of one phase stator

Manuscript received June 26, 2012; revised September 28, 2012 and November 14, 2012; accepted December 17, 2012. Date of publication January 9, 2013; date of current version February 7, 2013. This work was supported in part by the National Natural Science Foundation of China under Grant 51277077 and the Fundamental Research Funds for the Central Universities of China under Grant 11QG55. Paper no. TEC-00337-2012.

B. Xu and L. Sun are with the State Key Laboratory of Alternate Electrical Power System with Renewable Energy Sources, North China Electric Power University, Baoding 071003, China (e-mail: xbq_ncepu@126.com; sll_ncepu@126.com).

L. Xu and G. Xu are with the School of Electronics, Electrical Engineering and Computer Science, Queen's University Belfast, Belfast, BT9 5AH, U.K. (e-mail: l.xu@ee.qub.ac.uk; xu_gy@ncepu.edu.cn).

Color versions of one or more of the figures in this paper are available online at http://ieeexplore.ieee.org.

Digital Object Identifier 10.1109/TEC.2012.2236557

current for FFT analysis, yielding better frequency separation. Although it achieves significant improvement in detecting BRB at low slip, this method still depends on FFT and suffers from the long measurement time required (100 s in [15]), which induces extra distortion. Similarly, the Park's vector modulus, the envelope, the magnetic-torque current, the inverter input current (for inverter-fed motors), and the instantaneous power were used for FFT analysis to detect BRB in [16]–[22], respectively. Again, they are all inefficient at low slip and are less practical with respect to the Hilbert method due to the requirement of multiphase current and voltage signals.

To overcome this problem, the envelope and the instantaneous frequency of the left side band harmonic of the start-up stator current have been investigated in [23] and [24], respectively, both achieving satisfactory results. However, such techniques are confined to the start-up transient and inevitably suffer from the short duration time varying from only a fraction of a second up to several seconds.

Alternative high-frequency resolution techniques, such as multiple signal classification (MUSIC) [25]–[27] and estimation of signal parameters via rotational invariance technique (ESPRIT) [28]–[32], have been proposed to achieve satisfactory frequency resolution with a short measurement time. This can hopefully lead to avoiding the hindering variations of stator current and slip in the measurements. In [33], [34], MUSIC was used to detect BRB with a short measurement time of 3 s; however, the issue of low slip was not addressed.

Based on the excellent work in [15] and [33], [34], this paper addresses the issue of detecting BRB at low slip by conjugating HT and ESPRIT, which is superior to MUSIC in both precision and reliability [35].

This paper is organized as follows. Section II recalls the Hilbert method and reveals the particular difficulties in detecting BRB in the case of low slip. Section III describes the basis of ESPRIT and its suitability for BRB detection at low slip. A novel detection method combining HT and ESPRIT is presented in Section IV. The experimental results of a small motor in a laboratory and a large motor operating on site are reported in Section V to demonstrate the effectiveness of the proposed method. Section VI gives some discussions, and finally, Section VII draws the conclusions.

II. Hilbert Method for BRB Detection

A. Theoretical Basis

The HT of a real signal $i_s(t)$, such as one phase the stator current, is mathematically defined as $\hat{i}_{\rm s}(t)$ [15]:

$$\hat{i}_{\rm s}(t) = \frac{1}{\pi}\int_{-\infty}^{+\infty}\frac{i_{\rm s}(\tau)}{t-\tau}d\tau. \tag{1}$$

By coupling $i_s(t)$ and $\hat{i}_{\rm s}(t)$, the so-called analytical signal $\bar{i}_{\rm s}(t)$ is created

$$\bar{i}_{\rm s}(t) = i_{\rm s}(t) + j\hat{i}_{\rm s}(t) \tag{2}$$

where j is the imaginary unit. The Hilbert modulus is defined as

$$M(t) = i_s^2(t) + \hat{i}_s^2(t). \tag{3}$$

An interesting property of HT as indicated by (1)–(3) is that the HT of a trigonometric function is a version of itself with a 90° phase shift, meaning that cosine is transformed to sine, and vice versa.

In the case of periodic disturbances produced by BRB, one phase stator current can be formulated by superimposing the $(1 \pm 2ks)f_1$ components ($k = 1, 2$, the other components with $k > 2$ are neglected due to their smaller magnitudes) to the fundamental one as [2]–[4], [15], [21]

$$\begin{aligned} i_{\rm s}(t) = {} & I_{\rm m1}\cos(2\pi f_1 t + \phi_1) \\ & + I_{\rm mL}\cos[2\pi(1-2s)f_1 t + \phi_{\rm L}] \\ & + I_{\rm mR}\cos[2\pi(1+2s)f_1 t + \phi_{\rm R}] \\ & + I_{\rm mLL}\cos[2\pi(1-4s)f_1 t + \phi_{\rm LL}] \\ & + I_{\rm mRR}\cos[2\pi(1+4s)f_1 t + \phi_{\rm RR}] \end{aligned} \tag{4}$$

where $I_{\rm m1}, I_{\rm mL}, I_{\rm mR}, I_{\rm mLL}, I_{\rm mRR}$ represent the magnitudes of the f_1, $(1-2s)f_1$, $(1+2s)f_1$, $(1-4s)f_1$, $(1+4s)f_1$ components, respectively, and ϕ_1, $\phi_{\rm L}$, $\phi_{\rm R}$, $\phi_{\rm LL}$, $\phi_{\rm RR}$ represent the corresponding initial phases.

The HT of this current can be constructed by changing the cosine functions for sine functions, and subsequently, the Hilbert modulus is obtained according to (3) as

$$\begin{aligned} M(t) = {} & i_{\rm s}^2(t) + \hat{i}_{\rm s}^2(t) \\ = {} & I_{\rm m1}^2 + I_{\rm mL}^2 + I_{\rm mR}^2 + I_{\rm mLL}^2 + I_{\rm mRR}^2 \\ & + 2I_{\rm m1}I_{\rm mL}\cos[2\pi(2s)f_1 t + \phi_1 - \phi_{\rm L}] \\ & + 2I_{\rm m1}I_{\rm mR}\cos[2\pi(2s)f_1 t + \phi_{\rm R} - \phi_1] \\ & + 2I_{\rm mL}I_{\rm mLL}\cos[2\pi(2s)f_1 t + \phi_{\rm L} - \phi_{\rm LL}] \\ & + 2I_{\rm mR}I_{\rm mRR}\cos[2\pi(2s)f_1 t + \phi_{\rm RR} - \phi_{\rm R}] \\ & + 2I_{\rm m1}I_{\rm mLL}\cos[2\pi(4s)f_1 t + \phi_1 - \phi_{\rm LL}] \\ & + 2I_{\rm m1}I_{\rm mRR}\cos[2\pi(4s)f_1 t + \phi_{\rm RR} - \phi_1] \\ & + 2I_{\rm mL}I_{\rm mR}\cos[2\pi(4s)f_1 t + \phi_{\rm R} - \phi_{\rm L}] \\ & + 2I_{\rm mL}I_{\rm mRR}\cos[2\pi(6s)f_1 t + \phi_{\rm RR} - \phi_{\rm L}] \\ & + 2I_{\rm mLL}I_{\rm mR}\cos[2\pi(6s)f_1 t + \phi_{\rm R} - \phi_{\rm LL}] \\ & + 2I_{\rm mLL}I_{\rm mRR}\cos[2\pi(8s)f_1 t + \phi_{\rm RR} - \phi_{\rm LL}]. \end{aligned} \tag{5}$$

Equation (5) indicates that $M(t)$ is a complicated combination of dc component and others at frequencies of $2sf_1, 4sf_1, 6sf_1$, and $8sf_1$. Considering the experiential knowledge that $I_{\rm m1} \gg I_{\rm mL}, I_{\rm m1} \gg I_{\rm mR}, I_{\rm mL} > I_{\rm mLL}, I_{\rm mR} > I_{\rm mRR}$ [2]–[10], the components at frequencies of $6sf_1$ and $8sf_1$ are negligible, and the Hilbert modulus can hence be simplified as

$$\begin{aligned} M(t) \approx {} & I_{\rm m1}^2 + I_{\rm mL}^2 + I_{\rm mR}^2 + I_{\rm mLL}^2 + I_{\rm mRR}^2 \\ & + 2I_{\rm m1}I_{\rm mL}\cos[2\pi(2s)f_1 t + \phi_1 - \phi_{\rm L}] \\ & + 2I_{\rm m1}I_{\rm mR}\cos[2\pi(2s)f_1 t + \phi_{\rm R} - \phi_1] \end{aligned}$$

$$+ 2I_{\mathrm{m1}} I_{\mathrm{mLL}} \cos[2\pi(4s)f_1 t + \phi_1 - \phi_{\mathrm{LL}}]$$
$$+ 2I_{\mathrm{m1}} I_{\mathrm{mRR}} \cos[2\pi(4s)f_1 t + \phi_{\mathrm{RR}} - \phi_1]. \quad (6)$$

This clearly shows that the two components at frequencies of $2sf_1$ and $4sf_1$ in the Hilbert modulus are both associated with BRB and can be treated as the BRB indicator. The dominating dc component is regarded as an intensive noise and needs to be minimized as much as possible.

Based on the previous discussion, the Hilbert method for BRB detection, as presented in [15], has the following basic steps.

1) Measure one phase stator current, labeled as $i_s(t)$.
2) Compute the HT of $i_s(t)$, labeled as $\hat{i}_s(t)$ (In practice, the HT is computed using an FFT-based procedure [36]).
3) Compute Hilbert modulus $M(t)$ according to (3).
4) Remove the dc component in $M(t)$ by subtracting its average, and label the result as $M(t)^*$, i.e., $M(t)^* = M(t) - \mathrm{mean}(M(t))$.
5) Obtain the spectrum of $M(t)^*$ using FFT, and investigate the BRB indicator, i.e., the components at frequencies of $2sf_1$ and $4sf_1$ in the spectrum.

B. Difficulties in BRB Detection at Low Slip

The Hilbert method has significant advantages compared with the MCSA-based methods [4]–[10], namely:

1) Spectral leakage of the dominating component (the dc component in the Hilbert modulus) can be avoided easily by subtracting its average prior to spectral analysis. On the contrary, the traditional methods, directly dealing with the stator current, have difficulties in depressing spectral leakage of the dominating component, i.e., the f_1 component in the stator current. For example, a self-adaptive filter, synchronously tracking the f_1 component in both magnitude and frequency, was used to counteract the f_1 component in [6] in order to avoid spectral leakage. It is rather complex but yet less effective and can even be completely inefficient at low slip.
2) The investigation on the low-frequency components at $2sf_1$ and $4sf_1$ makes it possible that the sampling rate of the Hilbert modulus can be decimated before FFT is performed, dramatically reducing the computation burden.

However, this method does have some difficulties in dealing with low slip cases. First of all, its effectiveness depends on the condition that the spectral leakage of the dc component can be avoided completely by subtracting the average of the Hilbert modulus [15]. According to (6), it can be easily concluded that $I_{\mathrm{mL}}, I_{\mathrm{mR}}, I_{\mathrm{mLL}}$, and I_{mRR} should be constant during the measurement so as to yield a constant dc component which can then be counteracted completely by subtracting the average of the Hilbert modulus. However, this method again suffers from the conflict between frequency resolution and measurement time, i.e., a high-frequency resolution is needed at low slip requiring a long measurement time with an increasing likelihood of stator current and slip variations. As a consequence of this, the Hilbert method becomes ineffective because these variations cannot be completely avoided in reality, especially over a long measurement time.

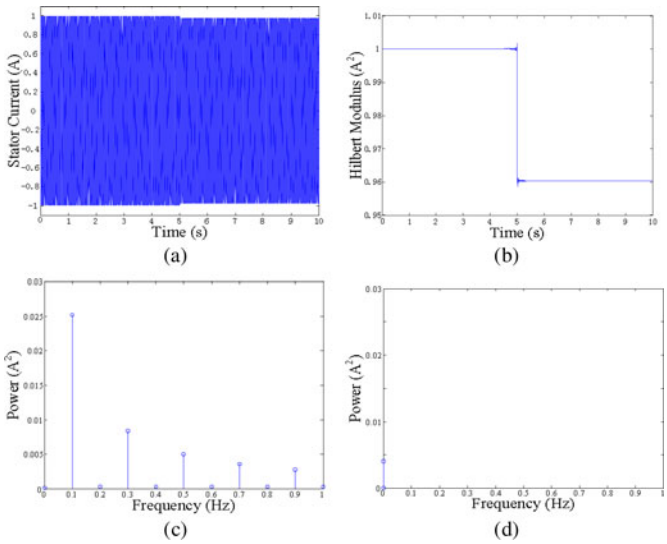

Fig. 1. Simulated results with stator current variation. (a) Stator current profile. (b) Hilbert modulus. (c) FFT spectrum. (d) ESPRIT spectrum.

TABLE I
SIMULATED SPECIFICATIONS WITH STATOR CURRENT VARIATION

Variable	Value	
	Time interval 0~5s	Time interval 5~10s
f_1 (Hz)	50.0	50.0
I_{m1} (A)	1.00	0.98
φ_1	π/6	π/6

Fig. 1(a)–(c) presents the waveforms of the stator current simulated using (4) with the specifications shown in Table I, the Hilbert modulus, and its FFT spectrum, respectively. In this case, $I_{\mathrm{mL}}, I_{\mathrm{mR}}, I_{\mathrm{mLL}}$, and I_{mRR} all equal zero, indicating that no BRB is present. However, I_{m1} has a 2% amplitude change in the middle of the measurement, commonly seen in practical conditions. This means that the dc component cannot be completely eliminated. Obviously, although BRB is not present, some peaks appeared in the spectrum arising from stator current variation, which are fairly close to $2sf_1$ or $4sf_1$, and can be easily misinterpreted as BRB indicator, leading to a false BRB diagnosis.

To overcome these problems, an improved Hilbert method using ESPRIT to replace FFT is proposed in the following sections.

III. ESPRIT FOR BRB DETECTION

A. Principles of ESPRIT

ESPRIT was originally developed by Roy *et al.* [28]–[31] and has been widely used to estimate the parameters (especially the frequencies) of cosinoidal signals [32]. The basic procedure of ESPRIT is briefly introduced in the following.

The measured signal can be written as

$$x(n) = \sum_{i=1}^{p} A_i \cos\left(2\pi f_i n T_{\mathrm{s}} + \varphi_i\right), \quad n=1,2,\ldots,N \quad (7)$$

where T_s is the sampling interval, N is the sampling number, and p is the number of harmonics. A_i, f_i, and φ_i represent the magnitude, frequency, and initial phase of the ith harmonic, respectively.

Set $y(n) = x(n+1)$ and the following $m \times N$ matrices ($m \gg p$) exist

$$\mathbf{X}(n) = [\, x(n) \quad x(n+1) \quad \cdots \quad x(n+m-1) \,]^{\mathrm{T}} \tag{8}$$

$$\mathbf{Y}(n) = [\, y(n) \quad y(n+1) \quad \cdots \quad y(n+m-1) \,]^{\mathrm{T}}. \tag{9}$$

The autocorrelation matrix of $\mathbf{X}(n)$ and the mutual-correlation matrix of $\mathbf{X}(n)$ and $\mathbf{Y}(n)$ can be given by

$$\mathbf{R}_{\mathrm{XX}} = \mathrm{E}\{\mathbf{X}(n)\mathbf{X}^{\mathrm{H}}(n)\} \tag{10}$$

$$\mathbf{R}_{\mathrm{XY}} = \mathrm{E}\{\mathbf{X}(n)\mathbf{Y}^{\mathbf{H}}(n)\} \tag{11}$$

where E and H represent mathematical expectation and conjugate transpose, respectively.

Based on the above definition, the procedure of using ESPRIT for calculating the frequency and amplitude can be summarized as follows.

1) Estimate the number of harmonics, p.
   Practically, one way to determine p is by empirically setting an initial value and then repeatedly adjusting it based on classification of eigenvalues of the autocorrelation matrix $\mathbf{R}_{\mathrm{XX}}$. In [33], an efficient algorithm that defines and minimizes a cost function for discrimination between the harmonics (corresponding to the p biggest eigenvalues) and noises has been successfully used to estimate p for MUSIC, and undoubtedly, can be applied to ESPRIT.
2) Determine the value of m.
   There is no theoretical basis to determine the exact value of m. However, as shown in [32], it can be empirically chosen as $m = (N - 2p)/3 + 2p$.
3) Construct the correlation matrices $\mathbf{R}_{\mathrm{XX}}$ and $\mathbf{R}_{\mathrm{XY}}$.
4) Calculate the minimum eigenvalue of $\mathbf{R}_{\mathrm{XX}}$, labeled as σ^2, and other eigenvalues.
5) Adjust the value of p by using the algorithm in [33], and then the value of m.
6) Calculate $\mathbf{R}_1 = \mathbf{R}_{\mathrm{XX}} - \sigma^2\mathbf{I}$, where $\mathbf{I}$ represents the $m \times m$ identity matrix.
7) Calculate $\mathbf{R}_2 = \mathbf{R}_{\mathrm{XY}} - \sigma^2\mathbf{Z}$, where $\mathbf{Z} = \begin{bmatrix} 0 & 0 \\ \mathbf{I}_{\mathrm{m}-1} & 0 \end{bmatrix}$ and $\mathbf{I}_{m}-1$ represents the $(m-1) \times (m-1)$ identity matrix.
8) Perform the singular decomposition of $\mathbf{R}_1$ as $\mathbf{R}_1 = \mathbf{U}\mathbf{\Lambda}\mathbf{V}^{\mathrm{H}}$, where $\mathbf{U} = [\mathbf{U}_1\ \mathbf{U}_2]$, $\mathbf{V}^{\mathrm{H}} = \begin{bmatrix} \mathbf{V}_1^{\mathrm{H}} & \mathbf{V}_2^{\mathrm{H}} \end{bmatrix}^{\mathrm{T}}$, and $\mathbf{\Lambda} = \begin{bmatrix} \mathbf{\Lambda}_1 & 0 \\ 0 & \mathbf{\Lambda}_2 \end{bmatrix}$ ($\mathbf{\Lambda}_1$ is composed of the p main singular value).
9) Calculate $\mathbf{U}_1^{\mathrm{H}}\mathbf{R}_2\mathbf{V}_1$.
10) Calculate the p generalized eigenvalues of $\{\mathbf{\Sigma}_1,\ \mathbf{U}_1^{\mathrm{H}}\mathbf{R}_2\mathbf{V}_1\}$, $\lambda_i (i = 1, 2, \ldots, p)$, and all the other $(m-p)$ generalized eigenvalues equal zero.
11) Determine the frequencies as $f_i = (2\pi)^{-1}\tan^{-1}$ [Im(λ_i)/Re(λ_i)], where Re(λ_i) and Im(λ_i) represent the real and imaginary part of the eigenvalue λ_i, respectively.
12) Calculate

$$\lambda = \begin{bmatrix} 1 & 1 & \cdots & 1 \\ \lambda_1 & \lambda_2 & \cdots & \lambda_p \\ \vdots & \vdots & \ddots & \vdots \\ \lambda_1^{N-1} & \lambda_2^{N-1} & \cdots & \lambda_p^{N-1} \end{bmatrix}.$$

13) Calculate $\mathbf{c} = (\lambda^H\lambda)^{-1}\lambda^H\mathbf{X}$, where $\mathbf{c}$ and $\mathbf{X}$ are both column vectors and are expressed as $\mathbf{c} = [c_1 c_2 \ldots c_p]^T$ and $\mathbf{X} =$

$$[\, x(1) \quad x(2) \quad \cdots \quad x(N) \,]^{\mathrm{T}}.$$

14) Determine the amplitudes as $A_i = 2\,|c_i|\,, i = 1, 2, \ldots, p$.
   Detailed information of ESPRIT can be found in [28]–[32], especially in [32], which summarized the theoretical background and the procedure of ESPRIT and discusses the selection of the parameters of ESPRIT, such as N, p, and m.

B. Applying ESPRIT to detect BRB

Corresponding to the simulated stator current with the specifications in Table I, the ESPRIT spectrum of the Hilbert modulus is given in Fig. 1(d). Compared to Fig. 1(c), there are no peaks close to $2sf_1$ or $4sf_1$, thus eliminating the possibility of misinterpreting the stator current variation as BRB. This is ascribed to the capability of ESPRIT to avoid spectral leakage due to the fact that ESPRIT is based on the calculation of correlation matrices, eigenvalues, and singular decomposition.

On the other hand, such capability is not unlimited. A series of tests has been conducted with varying stator current and the corresponding results demonstrate that ESPRIT always performs well for variation not exceeding 2%.

IV. Improved Hilbert Method for BRB Detection

An improved detection method for BRB in induction motors is proposed by combining ESPRIT with the traditional Hilbert method. The basic steps used are as follows.

1) Measure the stator current, labeled as i_s, with a sampling frequency of 1 kHz and a period of 20 s.
   Note that the sampling frequency can be empirically determined, e.g., 10 kHz as in [15], or higher/lower according to specific requirements. In this paper, the frequencies of interest are f_1, $(1-2s)f_1$ and $(1+2s)f_1$, which are all around 50 Hz. Thus, a sampling frequency of 1 kHz, approximately 20 times of them, is used.
2) Analyze the RMS trend of i_s to extract the most steady part of i_s with a duration time slightly longer than $1/(2sf_1)$, labeled as i_s^s.
   This step is useful to avoid stator current variation. Naturally, the duration time should be as short as possible to minimize such variation. On the other hand, from signal processing perspective, the duration time should be at least a full cycle of the investigated signal so as to include its full information. As the BRB indicators have cycles of $1/(2sf_1)$ and $1/(4sf_1)$, the duration time should be set at least $1/(2sf_1)$. As for the supply frequency f_1 and the slip

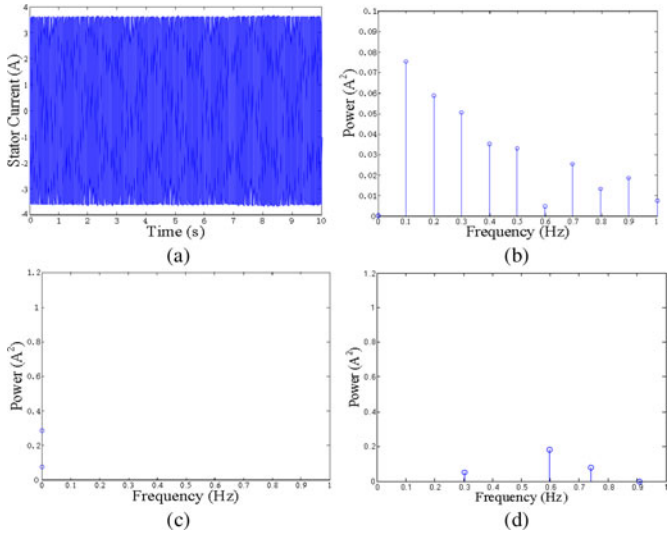

Fig. 2. Experiment results under the healthy condition. (a) Stator current profile. (b) FFT spectrum. (c) ESPRIT spectrum. (d) MUSIC spectrum.

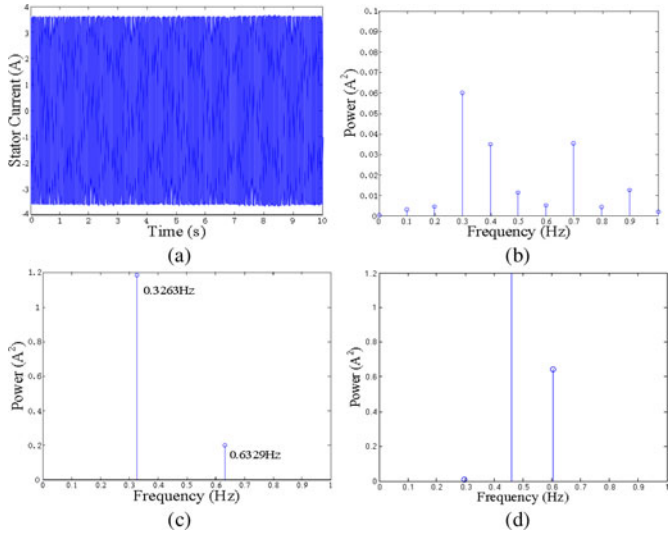

Fig. 3. Experiment results under the faulty condition. (a) Stator current profile. (b) FFT spectrum. (c) ESPRIT spectrum. (d) MUSIC spectrum.

s, they can be estimated by performing subdivision FFT on the stator current and subsequent investigation into the fundamental component and the rotor slot harmonics, as demonstrated in [6].

As for the RMS sequence of i_s, it can be easily calculated by using the well-known sliding window algorithm given by

$$I(k) = \sqrt{\frac{1}{M_w} \sum_{j=(k-1)M_w+1}^{k\,M_w} [i_s(j)]^2} \tag{12}$$

where M_w is the window size or sample number of a window and $i_s(j)$ is the jth sampled current [37].

Subsequently, a fitness function is defined as

$$f_{\text{fit}} = \sum [I(n) - I_{\text{av}}]^2 \tag{13}$$

where I_{av} is the overall average of the RMS sequence $I(k)$, and $I(n)$ is a certain part of $I(k)$ stretching over the prespecified duration time. Thus, by minimizing f_{fit}, the most steady part of i_s can be extracted in the meaning of least squares.

3) Compute the HT of i_s^s, labeled as $\hat{i}_s^s$.
4) Compute Hilbert modulus M as $M = (i_s^s)^2 + \left(\hat{i}_s^s\right)^2$.
5) Remove the dc component of M, leading to the difference $M^* = M - \text{mean}(M)$.
6) Down sample M^* with a suitable decimation factor to reduce computation burden, while maintaining a sampling frequency at least 20 times of $4sf_1$.
   Noting that it is important to apply a well-designed low-pass filter, such as a second-order Butterworth low-pass filter, to retain the $2sf_1$ and $4sf_1$ components and attenuate other noninterested components.
7) Perform spectral analysis with ESPRIT instead of FFT.
8) Diagnose whether BRB occurs according to the criterion: if both the two peaks at $2sf_1$ and $4sf_1$ appear, BRB is present.
9) Similar to [15], an index is introduced as $k_f = P_{2sf1}/I_{\text{m1}}^2$, and compared with the corresponding threshold in order to quantitatively evaluate the BRB severity, where P_{2sf1} represents the amplitude of the $2sf_1$ peak in the ESPRIT spectrum. As for the threshold, it can be predetermined by using the so-called case-study-based self-tuning technique [6].

V. Experimental Results

Using the test rig described in [10], various tests on an induction motor rated at 3 kW, 380 V/50 Hz, 2880 r/min have been carried out to validate the improved detection method.

Tests were carried out under healthy and faulty conditions with BRB. In both cases, the tests were performed under no-load condition to keep a low slip of around 0.0033.

First, one phase stator current over a 10-s period was analyzed using the traditional Hilbert method and the improved method, respectively. Also, an alternative method combining MUSIC and HT was also applied for comparison.

Under healthy conditions, Fig. 2 shows the phase stator current and the spectra obtained using the FFT, ESPRIT, and MUSIC respectively. For comparison, Fig. 3 gives the corresponding results under faulty conditions. Here, the sampling frequency is reduced from 1 kHz to 100 Hz. For the ESPRIT and MUSIC, p is estimated to be 13 and 15, respectively, for the healthy and faulty conditions. In order to avoid the possible underestimation of p, $p = 18$ is used for both conditions and $N = 643$ and $m = 357$.

As shown in Fig. 2(b), although the motor is healthy, the FFT spectrum has two peaks at 0.3 and 0.7 Hz, which are close to $2sf_1$ (≈0.33 Hz) or $4sf_1$ (≈0.66 Hz). Hence, it is likely that those two peaks could be misinterpreted as the BRB indicator, leading to a false diagnosis. In contrast, Fig. 2(c) using ESPRIT

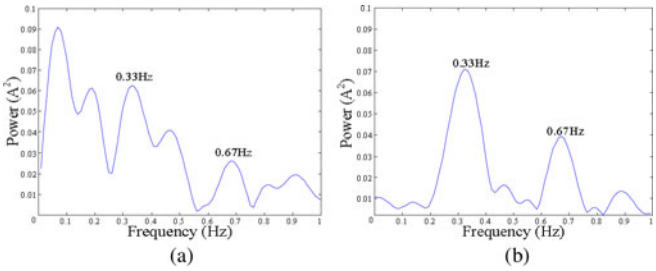

Fig. 4. FFT spectra over a 100 s measurement. (a) Healthy condition. (b) Faulty condition.

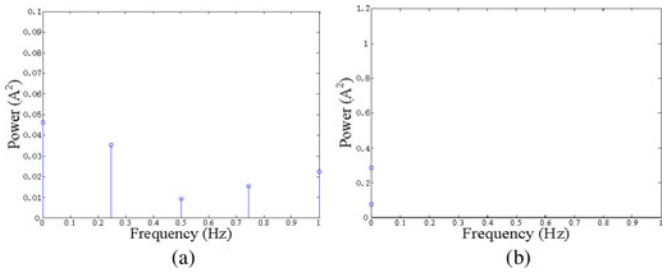

Fig. 5. Experiment results with a shorter measurement under the healthy condition. (a) FFT spectrum. (b) ESPRIT spectrum.

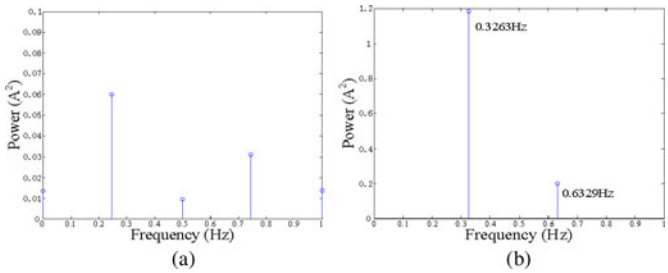

Fig. 6. Experiment results with a shorter measurement under the faulty condition. (a) FFT spectrum. (b) ESPRIT spectrum.

Fig. 7. Motor incipient failure online detector.

only has a few peaks around 0 Hz. As they are located far away from $2sf_1$ and $4sf_1$, it eliminates the possibility of false diagnosis.

Fig. 3(b) demonstrates that the FFT spectrum under the faulty condition does detect the two components at 0.3 and 0.7 Hz. However, it has the following drawbacks due to the limitations of spectral leakage and frequency resolution.

1) The spectrum contains other peaks which can cause confusion to the BRB detection.
2) It can only present the peaks at multiple frequencies of the frequency resolution, i.e., 0.1 Hz in this example.

On the contrary, Fig. 3(c) shows that the ESPRIT spectrum presents only the BRB indicator at the precise frequencies of 0.3263 and 0.6329 Hz as expected, thus making it easier to provide a correct diagnosis.

The results shown so far clearly indicate improved performance by combining the traditional Hilbert method with ESPRIT. However, the attempt using MUSIC has failed to produce satisfactory results. The MUSIC spectrum shown in Fig. 2(d) under the healthy condition presents an incorrect BRB indicator and leads a false diagnosis. Under the faulty condition, the MUSIC spectrum shown in Fig. 3(d) presents a pseudopeak which can make the diagnosis ambiguous. In addition, MUSIC requires much more computational time than ESPRIT, 3.08 s versus 0.57 s, with the 10 s measurement data. Therefore, ESPRIT appears more preferable to MUSIC for improving the conventional Hilbert method.

To further validate the improved method, the FFT spectra over a 100 s measurement with a frequency resolution of 0.01 Hz are given in Fig. (4).

Similarly to Fig. 2(b), although the frequency resolution is greatly enhanced, Fig. 4(a) still exhibits two peaks at 0.33 and 0.67 Hz. Due to the enhanced frequency resolution, Fig. 4(b) does correctly present the true BRB indicator under the faulty condition.

By comparing Fig. 2(c) with Fig. 4(a), it is easy to conclude that the improved method can eliminate the kind of misinterpretation previously discussed. In the meantime, the comparison between Figs. 3(c) and 4(b) shows a satisfactory agreement in terms of the BRB indicator, demonstrating that the improved method is effective at detecting BRB.

Second, in the light of ESPRIT's high-frequency resolution, even with a short measurement time, further tests with the most steady part of stator current over a short period of 4 s, being slightly longer than $1/(2sf_1)$ of 3.3 s, have been carried out and the results under the healthy and faulty conditions are given in Figs. 5 and 6, respectively. For ESPRIT, the considered values are $p = 18$, $N = 243$, and $m = 157$.

Comparing Figs. 5(a) and 6(a), it can be seen that the two FFT spectra under the healthy and faulty conditions with 4 s measurement are similar, indicating the ineffectiveness of the traditional Hilbert method due to the low-frequency resolution of 0.25 Hz. On the other hand, the ESPRIT spectra given in Figs. 5(b) and 6(b) exhibit significant difference, proving the effectiveness of the improved Hilbert method. In fact, the two ESPRIT spectra are identical to the results obtained earlier with a 10 s measurement shown in Figs. 2(c) and 3(c), respectively. This demonstrates ESPRIT's unique capability of achieving a high-frequency resolution using a short period measurement, and thus, it is ideal to improve the BRB detection while avoiding possible disturbances caused by stator current variation.

The proposed method combining the HT and ESPRIT has been integrated into a portable instrument, "Motor Incipient Failure Online Detector," developed by the authors and shown in Fig. 7. It is used to detect BRB in large motors on industrial sites. As an example, a detection conducted on a large motor is presented here. This motor, rated at 2800 kW, 6 kV/340 A,

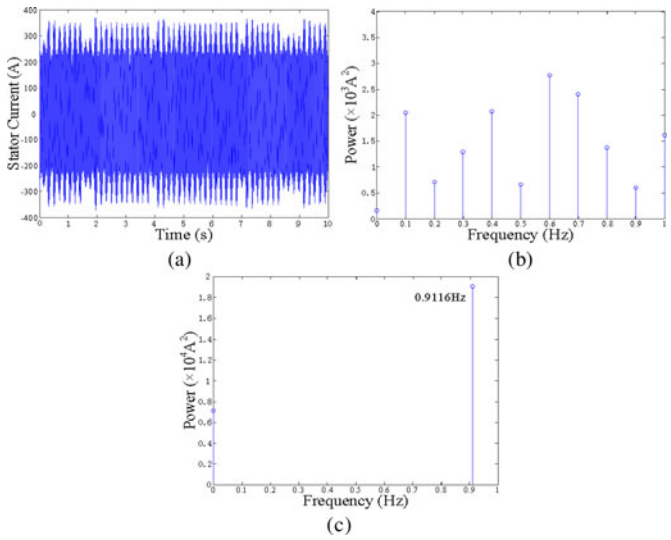

Fig. 8. Detection results of a large motor on site. (a) Stator current profile. (b) FFT spectrum. (c) ESPRIT spectrum.

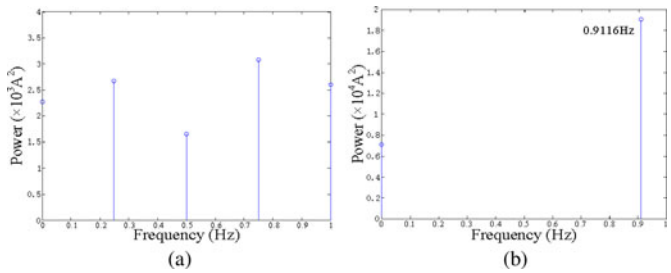

Fig. 9. Detection results of a large motor on site with a shorter measurement. (a) FFT spectrum. (b) ESPRIT spectrum.

331 r/min, and 50 Hz, is used in an oil refinery to drive a compressor. The motor normally operates at low slip of less than 0.007.

A 10 s measurement was initially used to give the detection results: Fig. 8 illustrates the profile of one phase stator current, as well as the FFT and ESPRIT spectra. A 4 s measurement was then used to yield the corresponding FFT and ESPRIT spectra shown in Fig. 9.

Fig. 8(a) portrays the stator current waveform with envelopes showing some punches, implying the presence of BRB or other abnormities [18]. Meanwhile, by analyzing the stator current using the method shown in [6], the supply frequency and the slip can both be estimated as $f_1 \approx 50$ Hz, $s \approx 0.0036$. The frequencies of interest can hereby be determined as $2sf_1 \approx 0.36$ Hz and $4sf_1 \approx 0.72$ Hz.

As shown in Fig. 8(b), the FFT spectrum shows two peaks at 0.4 and 0.8 Hz, which approximate to $2sf_1$ and $4sf_1$, respectively, and are likely to be regarded as the BRB indicator, thus resulting in the diagnosis of BRB present. This seems to be reasonable especially with the surged envelopes in the stator current waveform. However, maintenance engineers discovered that the rotor is actually healthy whereas the external driving system is abnormal. Obviously, the traditional Hilbert method would lead a false diagnosis. In contrast, the ESPRIT spectrum, shown in Fig. 8(c), only exhibits one peak at 0.9116 Hz which is far away from $2sf_1$ and $4sf_1$. Thus, it would conclude that there is no BRB indicator presenting in the ESPRIT spectrum and the rotor is healthy.

As for the FFT spectrum with a 4 s measurement, shown in Fig. 9(a), it is doubtful that this spectrum could provide the required detection due to the low-frequency resolution of 0.25 Hz. The mandatory use of such spectrum could again lead to a false diagnosis. In contrast, the ESPRIT spectrum shown in Fig. 9(b) is almost identical to Fig. 8(c) with 10 s measurement and thus provides the correct diagnosis.

VI. Discussions

This paper proposes a variant of the Hilbert modulus method previously presented in [15] for detecting BRB at low slip. The main improvements of this paper compared to [15] are summarized as follows.

1) It gives a generalized analytical expression of the Hilbert modulus.
   In [15], one phase stator current in case of BRB is assumed as
   $$I_m cos(\omega t) + \frac{\beta I_m}{2}\{\cos[(\omega-\omega_0)t] + \cos[(\omega+\omega_0)t]\} \tag{14}$$
   where, $\omega = 2\pi f_1$ and $\omega_0 = 2\pi s f_1$; I_m represents the magnitude of the f_1 component; β denotes the modulation index.
   Thus, it takes the false assumption that all the three components have the same initial phase of 0 and the two components associated with BRB have the same amplitude of $\beta I_m/2$. On the other hand, the one phase stator current represented in (4) provides a general analytical expression of the Hilbert modulus where (14) can be regarded as a special case.
2) More significantly, it combines HT with ESPRIT to achieve significant improvements.
   In this paper, ESPRIT rather than FFT in [15] is used to obtain the spectrum of the Hilbert modulus. Not only can the spectral leakage of dc component in the Hilbert modulus be avoided, but also high-frequency resolution is achieved even with a short measurement time. Thus, it provides an improved Hilbert modulus method for detecting BRB at low slip.

The improved method is superior over that presented in [15] in terms of the BRB detection performance though extra computational time is required for ESPRIT compared to FFT. For instance, a whole ESPRIT procedure with a 4 s measurement data on a Lenovo ThinkPad X100e laptop (CPU: AMD 1.6 GHz, Memory: 768 MB) takes about 0.34 s compared to 0.01 s with an FFT procedure. However, it is undoubted that the improved method is feasible for those laptop-based portable instruments, such as the Motor Incipient Failure Online Detector shown in Fig. 7. In addition, it is also feasible to implement the proposed method in DSP-based systems which are widely used for monitoring and controlling motors. In fact, the computational capability of a mainstream DSP, such as the TMS320C6678 integrated with eight cores running at up to 10 GHz and equipped

with up to 8 GB extended memory, is not less than the common laptops such as Lenovo ThinkPad X100e.

VII. Conclusion

This paper investigates the Hilbert method, previously used to detect BRB in induction motors. It finds that this method suffers from its inherent limitations of spectral leakage and the confrontation between frequency resolution and measurement time due to the use of FFT. Its effectiveness deteriorates or even completely fails for motors operating at low slip. During low slip operation, a high-frequency resolution is needed to correctly identify the BRB indicator, requiring a long measurement time. This in reality would inevitably include stator current variation, thus making it difficult to avoid spectral leakage of the dc component in Hilbert modulus. To overcome this, FFT is replaced by ESPRIT in this paper to take advantage of ESPRIT's ability to avoid spectral leakage and to achieve high-frequency resolution even with a short measurement time. Thus, an improved Hilbert method is presented by combining the HT and ESPRIT together. Experimental results of a small motor in a laboratory and a large motor operating on an industrial site demonstrate the effectiveness and superiority of the improved Hilbert method, over the traditional one, in the case of low slip. This improved method is quite promising for detecting BRB in low slip large motors widely used in industrial applications.

References

[1] P. Zhang, Y. Du, T. G. Habetler, and B. Lu, "A survey of condition monitoring and protection methods for medium-voltage induction Motors," *IEEE Trans. Ind. Appl.*, vol. 47, no. 1, pp. 34–46, Jan./Feb. 2011.

[2] S. Williamson and A. C. Smith, "Steady-state analysis of 3-phase motors with rotor-bar and end-ring faults," *IEE Proc. B Electr. Power Appl.*, vol. 129, no. 3, pp. 93–100, May 1982.

[3] H. A. Toliyat and T. A. Lipo, "Transient analysis of cage induction machines under stator, rotor bar and end ring faults," *IEEE Trans. Energy Convers.*, vol. 10, no. 2, pp. 241–247, Jun. 1995.

[4] N. M. Elkasabgy, A. R. Eastham, and G. E. Dawson, "Detection of broken rotor bars in the cage rotor on an induction machine," *IEEE Trans. Ind. Appl.*, vol. 28, no. 1, pp. 165–171, Jan./Feb. 1992.

[5] A. Bellini, F. Fillippetti, G. Franceschini, C. Tassoni, and G. B. Kliman, "Quantitative evaluation of induction motor broken bars by means of electrical signature analysis," *IEEE Trans. Ind. Appl.*, vol. 37, no. 5, pp. 1248–1255, Sep./Oct. 2001.

[6] B. Q. Xu, H. M. Li, and L. L. Sun, "Sensitive and reliable detection of broken rotor bar fault in induction motors," in *Proc. IEEE 39th IAS Annu. Meeting*, Seattle, WA, Oct. 3–7, 2004, vol. 2, pp. 714–719.

[7] H. Douglas, P. Pillay, and A. K. Ziarani, "Broken rotor bar detection in induction machines with transient operating speeds," *IEEE Trans. Energy Convers.*, vol. 20, no. 1, pp. 135–141, Mar. 2005.

[8] J. H. Jung, J. J. Lee, and B. H. Kwon, "Online diagnosis of induction motors using MCSA," *IEEE Trans. Ind. Electron.*, vol. 53, no. 6, pp. 1842–1852, Dec. 2006.

[9] M. C. Ian and R. Wendell, "Using current signature analysis technology to reliably detect cage winding defects in squirrel-cage induction motors," *IEEE Trans. Ind. Appl.*, vol. 43, no. 2, pp. 422–428, Mar./Apr. 2007.

[10] B. Q. Xu, L. L. Sun, and H. Ren, "A new criterion for the quantification of broken rotor bars in induction motors," *IEEE Trans. Energy Convers.*, vol. 25, no. 1, pp. 100–106, Mar. 2010.

[11] C. T. Kowalski and W. Kanior, "Effectiveness of the frequency analysis of the stator current in the rotor fault detection," in *Proc. IEEE Int. Conf. Ind. Technol.*, Chengdu, China, Apr. 21–24, 2008, pp. 1–5.

[12] A. Bellini, A. Yazidi, F. Fillippetti, C. Rossi, and G.-A. Capolino, "High frequency resolution for rotor fault of induction machines," *IEEE Trans. Ind. Electron.*, vol. 55, no. 12, pp. 4200–4209, Dec. 2008.

[13] A. Bouzida, O. Touhami, R. Ibtiouen, A. Belouchrani, M. Fadel, and A. Rezzoug, "Fault diagnosis in industrial induction machines through discrete wavelet transform," *IEEE Trans. Ind. Electron.*, vol. 58, no. 9, pp. 4385–4395, Sep. 2011.

[14] Y. Gritli, C. Rossi, L. Zarri, F. Filippetti, A. Chatti, and D. Casadei, "Double frequency sliding and Wavelet analysis for rotor fault diagnosis in induction motors under time-varying operating condition," in *Proc. IEEE 8th Int. Symp. Diagnostics Electr. Mach., Power Electron. Drives*, Bologna, Italy, Sep. 5–8, 2011, pp. 676–683.

[15] P. Puche-Panadero, M. Pineda-Sanchez, M. Riera-Guasp, J. Roger-Folch, E. Hurtado-Perez, and J. Perez-Cruz, "Improved resolution of the MCSA method via Hilbert transform, enabling the diagnosis of rotor asymmetries at very low slip," *IEEE Trans. Energy Convers.*, vol. 24, no. 1, pp. 52–59, Mar. 2009.

[16] A. Aboubou, M. Sahraoui, and S. E. Zouou, "Broken bars and/or end rings detection in three-phase induction motors by the extended Park's vector approach," in *Proc. IEEE 9th Int. Power Electron. Congr.*, Celaya, Mexico, Oct. 17–22, 2004, pp. 128–133.

[17] C. M. Pezzani, P. D. Donolo, A. M. Castellino, G. R. Bossio, and C. H. De Angelo, "A new approach to the Park's vector for broken bars and load oscillation diagnosis on IM," in *Proc. IEEE 9th Int. Conf. Ind. Technol.*, Viña del Mar, Chile, Mar. 14–17, 2010, pp. 1221–1226.

[18] A. M. da Silva, R. J. Povinelli, and N. A. O. Demerdash, "Induction machine broken bar and stator short-circuit fault diagnostics based on three-phase stator current envelopes," *IEEE Trans. Ind. Electron.*, vol. 55, no. 3, pp. 1310–1318, Mar. 2008.

[19] N. Hu, L. Xia, F. Gu, and G. Qin, "A novel transform demodulation algorithm for motor incipient fault detection," *IEEE Trans. Instrum. Meas.*, vol. 60, no. 2, pp. 480–487, Feb. 2011.

[20] I. P. Georgakopoulos, E. D. Mitronikas, and A. N. Safacas, "Detection of induction motor faults in inverter drives using inverter input current analysis," *IEEE Trans. Ind. Electron.*, vol. 58, no. 9, pp. 4365–4373, Sep. 2011.

[21] Z. Liu, X. Yin, and Z. Zhang, "Online rotor mixed fault diagnosis way based on spectrum analysis of instantaneous power in squirrel cage induction motors," *IEEE Trans. Energy Convers.*, vol. 19, no. 3, pp. 485–490, Sep. 2004.

[22] M. Drif and A. J. Marques Cardoso, "The use of the instantaneous-reactive-power signature analysis for rotor-cage-fault diagnostics in three-phase induction motors," *IEEE Trans. Ind. Electron.*, vol. 56, no. 11, pp. 4606–4614, Nov. 2009.

[23] R. Supangat, N. Ertugrul, W. L. Soong, D. A. Gray, C. Hansen, and J. Grieger, "Detection of broken rotor bars in induction motor using starting-current analysis and effects of loading," *IEE Proc.—Electr. Power Appl.*, vol. 153, no. 6, pp. 848–855, Nov. 2006.

[24] M. Pineda-Sanchez, M. Riera-Guasp, J. A. Antonino-Daviu, J. Roger-Folch, J. Perez-Cruz, and R. Puche-Panadero, "Instantaneous frequency of the left sideband harmonic during the start-up transient: A new method for diagnosis of broken bars," *IEEE Trans. Ind. Electron.*, vol. 56, no. 11, pp. 4557–4570, Nov. 2009.

[25] R. O. Schmidt, "Multiple emitter location and signal parameter estimation," *IEEE Trans. Antennas Propag.*, vol. 34, no. 3, pp. 276–280, Mar. 1986.

[26] Q. T. (Keith) Zhang, "Probability of resolution of the MUSIC algorithm," *IEEE Trans. Signal Process.*, vol. 43, no. 4, pp. 978–987, Apr. 1995.

[27] P. Stoica and A. Nehorai, "MUSIC, maximum likelihood, and Cramer-Rao bound: further results and comparisons," *IEEE Trans. Acoust., Speech, Signal Process.*, vol. 38, no. 12, pp. 2140–2150, Dec. 1995.

[28] R. Roy, A. Paulraj, and T. Kailath, "ESPRIT–A subspace rotation approach to estimation of parameters of cisoids in noise," *IEEE Trans. Acoust., Speech, Signal Process.*, vol. ASSP-34, no. 5, pp. 1340–1342, Oct. 1986.

[29] R. Roy and T. Kailath, "ESPRIT-estimation of signal parameters via rotational invariance techniques," *IEEE Trans. Acoust., Speech, Signal Process.*, vol. 37, no. 7, pp. 984–995, Jul. 1989.

[30] R. Roy and T. Kailath, "Performance analysis of the total least squares ESPRIT algorithm," *IEEE Trans. Signal Process.*, vol. 39, no. 5, pp. 1122–1135, May 1991.

[31] R. Roy and T. Kailath, "Prefiltering-based ESPRIT for estimating sinusoidal parameters in non-Gaussian ARMA noise," *IEEE Trans. Signal Process.*, vol. 43, no. 1, pp. 349–353, Jan. 1995.

[32] I. Y.-H. Gu and M. H. J. Bollen, "Estimating interharmonics by using sliding-window ESPRIT," *IEEE Trans. Power Del.*, vol. 23, no. 1, pp. 13–23, Jan. 2008.

[33] S. H. Kia, H. Henao, and G.-A. Capolino, "A high-resolution frequency estimation method for three-phase induction machine fault detection," *IEEE Trans. Ind. Electron.*, vol. 54, no. 4, pp. 2305–2314, Aug. 2007.

[34] A. Garcia-Perez, R. de Jesus Romero-Troncoso, E. Cabal-Yepez, and R. A. Osornio-Rios, "The application of high-resolution spectral analysis for identifying multiple combined faults in induction motors," *IEEE Trans. Ind. Electron.*, vol. 58, no. 6, pp. 2002–2010, May 2011.
[35] R. Roy, A. Paulraj, and T. Kailath, "Comparative performance of ESPRIT and MUSIC for direction-of-arrival estimation," in *Proc. IEEE Int. Conf. Acoust., Speech Signal Process.*, Dallas, TX, Apr. 6–9, 1987, pp. 2344–2347.
[36] L. Marple, Jr., "Computing the discrete-time analytic signal via FFT," *IEEE Trans. Signal Process.*, vol. 47, no. 9, pp. 2600–2603, Sep. 1999.
[37] M. Bollen, *Understanding Power Quality Problems: Voltage Sags and Interruptions*. New York: IEEE Press, 1999.

Boqiang Xu (M'05) received the Ph.D. degree from North China Electric Power University, Baoding, China, in 2003.

Since 1997, he has been with North China Electric Power University, where he is currently a Professor in the School of Electrical Engineering. His research interests include condition monitoring and fault diagnosis of electric machines.

Liling Sun received the Ph.D. degree from North China Electric Power University, Baoding, China, in 2008.

Since 1997, she has been with North China Electric Power University, where she is currently an Associate Professor in the School of Electrical Engineering. Her research interests include condition monitoring and fault diagnosis of electric machines.

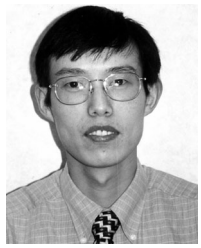

Lie Xu (M'03–SM'06) received the Ph.D. degree from the University of Sheffield, Sheffield, U.K., in 1999.

He is currently with the School of Electronics, Electrical Engineering and Computer Science, Queen's University Belfast, Belfast, U.K. His current research interests include power electronics, wind energy generation and grid integration, and application of power electronics to power systems.

Guoyi Xu received the M.Sc. degree in electrical engineering from North China Electric Power University, Baoding, China, in 2006. He is currently working toward the Ph.D. degree at Queen's University Belfast, Belfast, U.K.

He is also with the Key Laboratory of Power System Protection and Dynamic Security Monitoring, North China Electric Power University. His research interests include renewable power integration.